



Providing Choice & Value
Generic CT and MRI Contrast Agents



CONTACT REP

AJNR

Lesion-Filling Index from Quantitative DSA Correlates with Hemorrhage of Cerebral AVM

Ruinan Li, Yu Chen, Pingting Chen, Li Ma, Heze Han,
Zhipeng Li, Wanting Zhou, Xiaolin Chen and Yuanli Zhao





This information is current as
of July 19, 2025.

AJNR Am J Neuroradiol 2024, 45 (6) 712-720

doi: <https://doi.org/10.3174/ajnr.A8218>

<http://www.ajnr.org/content/45/6/712>

Lesion-Filling Index from Quantitative DSA Correlates with Hemorrhage of Cerebral AVM

 Ruinan Li,  Yu Chen, Pingting Chen,  Li Ma, Heze Han, Zhipeng Li, Wanting Zhou, Xiaolin Chen, and  Yuanli Zhao



ABSTRACT

BACKGROUND AND PURPOSE: Rupture is the most life-threatening manifestation of cerebral AVMs. This study aimed to explore the hemodynamic mechanism of AVM rupture. We introduced a new quantitative DSA parameter that can reflect the degree of intranidal blood stasis, called the lesion-filling index.

MATERIALS AND METHODS: This study examined patients with AVMs who had undergone both DSA and MR imaging between 2013 and 2014. Clinical presentations, angioarchitecture, and hemodynamic parameters generated from quantitative DSA were analyzed using univariate and multivariable logistic regression. The lesion-filling index was defined as the arterial diagnostic window divided by the volume of the AVM. To assess the correlation between the lesion-filling index and rupture, we incorporated the lesion-filling index into 2 published prediction models widely recognized for predicting AVM rupture risk, R₂eD and VALE. The DeLong test was used to examine whether the addition of the lesion-filling index improved predictive efficacy.

RESULTS: A total of 180 patients with AVMs were included. The mean lesion-filling index values in the ruptured group were higher compared with the unruptured group (390.27 [SD, 919.81] versus 49.40 [SD, 98.25]), $P < .001$. A higher lesion-filling index was significantly correlated with AVM rupture in 3 different multivariable logistic models, adjusting for angioarchitecture factors (OR = 1.004, $P = .02$); hemodynamic factors (OR = 1.005, $P = .009$); and combined factors (OR = 1.004, $P = .03$). Both R₂eD (area under the curve, 0.601 versus 0.624; $P = .15$) and VALE (area under the curve, 0.603 versus 0.706; $P < .001$) predictive models showed improved predictive performance after incorporating the lesion-filling index and conducting 10-fold cross-validation.

CONCLUSIONS: The lesion-filling index showed a strong correlation with AVM rupture, suggesting that overperfusion is the hemodynamic mechanism leading to AVM rupture.

ABBREVIATIONS: ADW = arterial diagnostic window; AUC = area under the curve; FWHM = full width at half maximum; LFI = lesion-filling index; QDSA = quantitative DSA; TRV = transnidal relative velocity

Cerebral AVMs involve abnormal tangles of brain arteries and veins, posing a risk of intracranial bleeding and neurologic issues. Among these symptoms, hemorrhage stands out as the

most life-threatening manifestation, remarkably affecting patients' quality of life.^{1,2} A comprehensive understanding of the mechanism of AVM rupture is crucial. Previous research has revealed that hemodynamics could play a pivotal role as a risk factor for rupture.³⁻⁵ The most influential early research was conducted by Spetzler et al,³ in 1992, in which they used micropipette direct puncture pressure measurement techniques to substantiate the impact of perfusion pressure on AVM rupture. Nevertheless, the intraprocedural puncture of feeding arteries, being an invasive procedure, entails certain risks and operational complexities. Consequently, contemporary research in hemodynamics now places greater emphasis on noninvasive investigative approaches.

Noninvasive hemodynamic measurement techniques such as quantitative DSA (QDSA) have been proved to assist in assessing rupture risk and planning treatments.⁵⁻¹⁰ QDSA is a medical imaging technique used to assess the structure and function of blood vessels. It builds on conventional DSA by providing

Received November 27, 2023; accepted after revision February 2, 2024.

From the Department of Neurosurgery (R.L., Y.C., L.M., H.H., Z.L., X.C., Y.Z.) and Beijing Neurosurgical Institute (Y.C., X.C., Y.Z.), Beijing Tiantan Hospital, Capital Medical University, Beijing, China; China National Clinical Research Center for Neurological Diseases (Y.C., X.C., Y.Z.), Beijing, China; College of Energy and Power Engineering (P.C.), Nanjing University of Aeronautics and Astronautics, Nanjing, China; Department of Neurological Surgery (L.M.), University of Pittsburgh Medical Center, Pittsburgh, Pennsylvania; and Department of Artificial Intelligence (W.Z.), Beijing University of Posts and Telecommunications, Beijing, China.

This study was supported by the Natural Science Foundation of China (82202244 to Yu Chen; 81771234 and 82071302 to Yuanli Zhao; 62376037 to Wanting Zhou) and the National Key R&D Program (2021YFC2501101, 2020YFC2004701 to Xiaolin Chen).

Ruinan Li and Yu Chen are co-first authors.

Please address correspondence to Yuanli Zhao, MD, Department of Neurosurgery, Beijing Tiantan Hospital, Beijing, 100070, P. R. China; e-mail: zhaoyuanli@126.com

 Indicates article with online supplemental data.

<http://dx.doi.org/10.3174/ajnr.A8218>

SUMMARY

PREVIOUS LITERATURE: Using quantitative digital subtraction angiography (QDSA) for the study of ruptured brain arteriovenous malformations, early recognition was associated with the mean transit time as published by Chen et al, correlating with silent intralesional microhemorrhages. Subsequent studies by Lin et al and Chen et al utilized QDSA-derived ROI curves, introducing a series of hemodynamic parameters strongly linked to rupture. These parameters were successfully employed in predicting AVM occlusion post-Gamma Knife treatment. While investigating the correlation between AVM rupture and hemodynamics, these studies concurrently demonstrated the valuable utility of QDSA parameters in the diagnosis and treatment of AVM.

KEY FINDINGS: We have found a novel QDSA hemodynamic parameter, Lesion-Filling Index (LFI), strongly correlated with AVM rupture.

KNOWLEDGE ADVANCEMENT: We discovered a novel QDSA hemodynamic parameter, designated as LFI, exhibiting a strong correlation with AVM rupture.

quantitative measurements of blood-flow dynamics. Previous studies had proposed several hemodynamic parameters associated with AVM rupture, such as MTT, the Stasis Index, and transnidus relative velocity (TRV), demonstrating the correlation of QDSA with AVM rupture^{6,9,11} However, regrettably, these parameters did not consider the supply arteries, draining veins, and the nidus as a unified entity in their hemodynamic analysis, somewhat compromising the reliability of these parameters.

Therefore, in this study, we propose the lesion-filling index (LFI), a new QDSA parameter that integrates the difference in filling between supply arteries and draining veins along with the nidus volume, embarking on a more holistic interpretation of hemodynamic-related hemorrhage.

MATERIALS AND METHODS

Study Design and Participants

This retrospective study was approved by Beijing Tiantan hospital institutional review board (KY 2020–003-01), adhering to Helsinki Declaration guidelines and STrengthening the Reporting of OBservational studies in Epidemiology (STROBE) reporting for observational case-control studies.

Patient Selection

To explore the connection between AVM hemodynamics and hemorrhagic presentation, we examined 384 consecutive brain AVMs between January 2013 and January 2014 from a single-center database registered in a nationwide multicenter registry. The MATCH registry (<https://clinicaltrials.gov/study/NCT04572568>), registered on ClinicalTrials.gov as NCT04572568, aimed to study the natural history and optimal individualized management strategy of AVMs in China. In this study, the inclusion criteria encompassed AVM diagnosis through DSA and/or MR imaging, with available preoperative DSA DICOM data. Exclusions were hereditary hemorrhagic telangiectasia, lack of preoperative DSA, and insufficient baseline information.

Study Parameters

We collected baseline characteristics, conventional DSA angioarchitecture, and QDSA parameters from all enrolled patients. All clinical parameters were assessed by 2 neurosurgeons with at least 5 years of clinical practice experience. All radiologic characteristics were independently evaluated by 2 credentialed senior neurointerventional

radiologists. If inconsistency existed, the final determination would be made by a professor of senior neurointerventional radiology with >30 years of clinical experience. Researchers who performed angioarchitecture and hemodynamic assessments were blinded to the clinical data.

Clinical baseline characteristics encompassed age on admission, sex, onset symptoms (hemorrhage, seizure, neurofunctional deficits, and others), and the mRS score on admission.

Angioarchitecture characteristics comprised the localization of AVMs, involvement of eloquent regions, and an array of features that had been analyzed in prior QDSA studies.^{7,12–15} Building on the angioarchitecture characteristics documented in prior literature, we investigated the following features in our study: dilation of feeding arteries, presence of single or multiple feeding arteries, categorization of venous drainage as either superficial or deep, identification of single or multiple venous drainage, assessment of draining venous stenosis, evaluation of nidus diffuseness, and identification of flow-related aneurysms. The definitions for these angioarchitecture features were aligned with the guidelines established by the American Society of Interventional and Therapeutic Neuroradiology.¹⁴ The definition of architecture characteristics is listed in the Online Supplemental Data.

QDSA parameters mainly refer to the hemodynamic parameters involved in previous QDSA-related studies and the quantitative hemodynamic parameters that can be calculated according to the fitted time-density curve, including the following: 1) TTP, 2) MTT, 3) full width at half maximum (FWHM), 4) arterial diagnostic window (ADW), 5) TRV, 6) the Stasis Index, and 7) LFI, and so forth.¹¹

DSA Acquisition and Quantitative Hemodynamics

All cases underwent the same DSA procedures with the same Axiom Artis angiosuite (Artis zee; Siemens) in our institution. The DSA standardized acquisition protocol is described in the Online Supplemental Data. For postprocessing of all QDSA data, syngo iFlow software (Siemens) was used.

In this study, certain hemodynamic parameters were defined with reference to previously published research.^{6,9,16} We chose the lateral view of common carotid angiography images to draw ROIs. For each patient, we investigated the following ROIs: 1) cavernous sinus segment of the ICA; 2) distal segment of the feeding artery; 3) AVM nidus; 4) proximal segment of the main

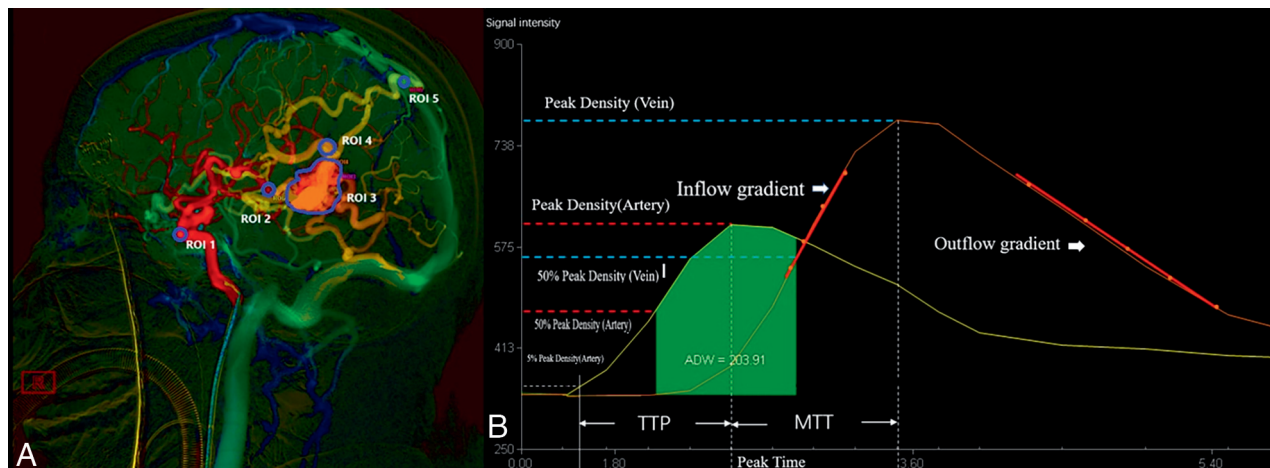


FIG 1. The time-density curve and color-coded QDSA. A, Lateral view of the color-coded QDSA. Selected ROIs are the following: 1) cavernous sinus segment of the ICA; 2) distal segment of the feeding artery; 3) AVM nidus; 4) proximal segment of the main draining vein; and 5) junction area of the draining vein and the venous sinus. B, Quantitative parameters in the time-density curve from QDSA. TTP indicates the time required for the bolus to reach peak attenuation, $ADW = \int_{T50\%A}^{T50\%V} A(t)dt$.

draining vein; and 5) junction area of the draining vein and venous sinus (Fig 1A).¹⁷ We used a standard circular ROI to delineate the supplying artery and draining vein characterized by the earliest contrast enhancement. For the AVM lesion, a polygonal tool was used to outline the ROI. The coordinates of time-density curves were measured by GetData Graph Digitizer (Version 2.24; S. Fedorov), and a customized program (Matlab; MathWorks) was used to fit the measured coordinate value (with the γ variable function, based on the least squares method) to get the standardized time-density curve.¹⁷

Gamma variable function : $C(t)$

$$= K(t - AT)^{\alpha} \times \exp [-(t - AT)/\beta].$$

$C(t)$ is the attenuation increment, t is the time after the start of contrast medium injection, K is a constant scale factor, α and β are fit coefficients, and AT (arrival time) is the time of arrival of the contrast medium.

The calculation formulas involving the parameters above were as follows (Fig 1B): TTP indicates the time required for the bolus to reach peak attenuation; MTT, the duration between peak attenuation of different ROIs; FWHM, the duration of the time-density curve rising to 50% peak attenuation and falling

to 50% peak attenuation; $ADW = \int_{T50\%A}^{T50\%V} A(t)dt$, calculated from the area under the curve (AUC) of the feeding arterial signal from Time (50% maximal arterial signal) to Time (50% maximal venous signal); TRV, maximum diameter (nidus)/FWHM; Stasis Index, inflow gradient/outflow gradient; LFI, ADW/volume (nidus).

Measurements of the Nidus

All enrolled patients underwent 1.5T or 3T MR imaging in our center. The maximum diameter was the greatest distance between 2 points within the AVM nidus, using MR imaging in the plane that most accurately depicted the largest cross-sectional area of

the AVM. To calculate the volume of nidus, we used the ellipsoid volume formula, which assumes that the AVM shape is approximately ellipsoidal in nature. The formula is

$$V = 4/3 \pi abc.$$

V is the volume of the nidus, and a , b , and c are the lengths of 3 perpendicular axes (measurements) of the nidus.

Statistical Analysis

Statistical analysis was performed using SPSS software (Version 26.0; IBM) and MedCalc for Windows (Version 22.013; MedCalc Software). For categorical variables, we presented frequencies and percentages, using the Pearson χ^2 test, Fisher exact test, and the Kruskal-Wallis ANOVA test for comparisons. Continuous variables were evaluated on the basis of normality assessment, using the independent Student t test or Mann-Whitney U rank-sum test as appropriate.

Univariate and multivariable logistic regression analyses were performed to calculate ORs and 95% CIs to identify predictors of hemorrhage in baseline characteristics, angioarchitecture, and hemodynamic features. The DeLong test was used to assess the statistically significant difference in the area under the receiver operating characteristic curve among the compared models. We selected 2 models, R₂eD (<https://www.ahajournals.org/doi/10.1161/STROKEAHA.119.025054>) and VALE (<https://jamanetwork.com/journals/jamanetworkopen/fullarticle/2801834>), from previously published studies known for their high correlation with AVM rupture.^{18,19} The R₂eD system incorporates factors such as AVM size, deep venous drainage, nidus location, race, and mono-arterial feeding. Meanwhile, the VALE system considers ventricular system involvement, venous aneurysm, deep location, and exclusively deep drainage. We further supplemented these 2 models by adding LFI to investigate its additive value associated with rupture. Performance of these models was evaluated using 10-fold cross-validation.

All *P* values were 2-sided, and statistical significance was considered at *P* < .05.

RESULTS

Baseline Characteristics

A total of 180 patients met the inclusion criteria and were included in this study (Fig 2). No significant differences in age, sex, and Spetzler-Martin grade distribution were observed between the ruptured (*n* = 103) and the unruptured (*n* = 77) groups. In comparison, ruptured AVMs often had higher mean mRS scores on admission (1.2 [SD, 1.3] versus 0.8 [SD, 0.6], *P* = .002) and were less prone to patients experiencing concurrent seizure symptoms (16.5% versus 41.6%, *P* < .001) (Table 1).

Differences in Hemodynamic and Angioarchitecture Characteristics

To identify the risk factors associated with hemorrhage, we performed a comparative analysis of angioarchitecture and hemodynamic characteristics between cases of unruptured and ruptured AVMs (Table 2). The mean nidus volume, a key indicator of AVM size, was significantly larger in unruptured cases compared with ruptured cases (40.2 [SD, 46.4] mL versus 13.6 [SD, 21.0] mL, *P* < .001).

In terms of angioarchitecture, several notable differences were observed. The unruptured group had a higher prevalence of

feeding artery dilation (74.0% versus 49.5%, *P* = .001), while the ruptured group had a higher incidence of a single feeding artery (34.0% versus 15.6%, *P* = .003). Other characteristics such as deep venous drainage, single draining vein, drainage vein stenosis, diffuse nidus, and flow-related aneurysms were also compared; however, no significant differences were found between the 2 groups.

Regarding hemodynamics, we examined various parameters for feeding arteries and drainage veins. While some differences were observed, including the FWHM, these did not reach statistical significance. Additionally, the study evaluated MTT (*P* = .017) and TRV (*P* < .001), both of which were significantly different between the two groups. LFI also showed a substantial difference (*P* < .001).

Association of LFI and Risk of AVM Rupture at Presentation in Hemodynamic, Angioarchitecture, and Combined AVM Models

To assess the statistical power and stability of the association between LFI and AVM rupture, we conducted several logistic regression analyses with LFI incorporated separately into the 3 models: hemodynamics, angioarchitecture, and a combined model. In the univariable analysis, LFI exhibited a significant association with AVM rupture risk (OR, 1.007; 95% CI, 1.003–1.010; *P* = .001). Similarly, in the angioarchitecture model, LFI remained significantly associated with rupture risk (OR, 1.004; 95% CI, 1.001–1.008; *P* = .02). The hemodynamic model also showed a significant association between AVM rupture and LFI (OR, 1.005; 95% CI, 1.001–1.009; *P* = .009). The combined model, which incorporates both angioarchitecture and hemodynamic factors, demonstrated a statistically significant association between AVM rupture and LFI as well (OR, 1.004; 95% CI, 1.000–1.007; *P* = .03) (Table 3). Notably, deep venous drainage, diffuse nidus, and flow-related aneurysms had significant associations with AVM rupture risk in the angioarchitecture model. All variables in the logistic regression had variance inflation factor values below the threshold of 10, demonstrating the absence of significant multicollinearity concerns.

Overall, these findings underscore the importance of LFI as a risk factor of AVM rupture, with consistent significance across various models.

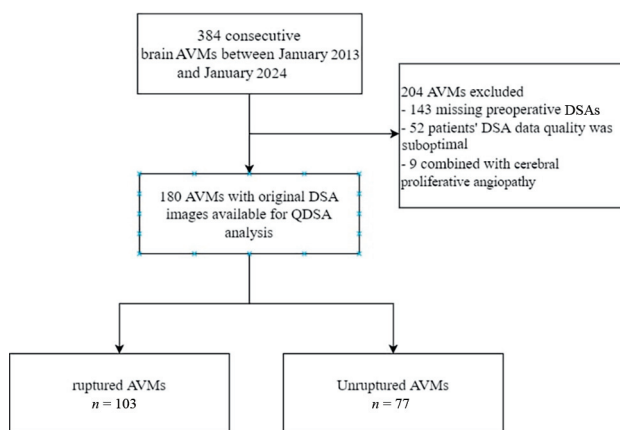


FIG 2. Flow diagram of the enrolled patients.

Table 1: Baseline characteristics

Characteristics	All Cases	Unruptured	Ruptured	<i>P</i> Value
No. of patients	180	77	103	
Age (mean) (yr)	24.6 (SD, 12.7)	25.2 (SD, 11.9)	24.2 (SD, 13.3)	.60
Sex (male)	110 (61.1%)	50 (64.9%)	60 (58.3%)	.22
Admission mRS score (mean)	1.0 (SD, 1.1)	0.8 (SD, 0.6)	1.2 (SD, 1.3)	.002 ^a
Clinical presentation				
Seizure	49 (27.2%)	32 (41.6%)	17 (16.5%)	<.001 ^a
Headache (nonruptured)	25 (13.9%)	24 (31.2%)	1 (1.0%)	<.001 ^a
Focal neurologic deficit	20 (11.1%)	12 (15.6%)	8 (7.8%)	.08
Spetzler-Martin grade				.07
I	30 (16.7%)	8 (10.4%)	22 (21.4%)	
II	61 (33.9%)	26 (33.8%)	35 (34.0%)	
III	53 (29.4%)	25 (32.5%)	28 (27.2%)	
IV	28 (15.6%)	15 (19.5%)	13 (12.6%)	
V	8 (4.4%)	3 (3.9%)	5 (4.9%)	

^a Statistical significance (*P* < .05).

Additive Value Assessment of LFI in the Previous Models

LFI has been established as a stable and robust risk factor of rupture in multivariate logistic regression analyses. To further assess its effectiveness, we incorporated LFI as a parameter into the previously published AVM rupture-risk scoring systems, such as the R₂eD and VALE score systems, and observed whether LFI enhances the predictive performance of the model.^{18,19}

We adjusted variables with statistically significant differences identified in the univariate analysis presented in

Table 2. We aimed to explore the stable relationship between LFI and rupture. Thus, 3 multivariable logistic regressions were performed to adjust for angioarchitectural, hemodynamic, and both factors. The selection of confounders was based on exploratory analysis using logistic regression (Table 2). Due to the cross-sectional nature of this study, there were inherent population differences, and some parameters in our study may differ from those in models such as R₂eD and VALE.

In the initial analysis, the R₂eD model exhibited an AUC of 0.755 (95% CI, 0.684–0.826), serving as the reference model. After the inclusion of LFI, the AUC for the R₂eD + LFI model increased to 0.791 (95% CI, 0.725–0.857), indicating a statistically significant improvement ($P = .03$) (Fig 3A). Additionally, LFI itself demonstrated significance as an independent risk factor (OR, 1.004; 95% CI, 1.000–1.008; $P = .04$).

Similarly, the VALE model, with an initial AUC of 0.760 (95% CI, 0.689–0.831) served as another reference model. After the inclusion of LFI, the VALE + LFI model showed a significant enhancement in discriminatory power, with an AUC of 0.823 (95% CI, 0.762–0.884) and a P value of .005 (Fig 3B). LFI, when added to the VALE model, was also found to be a significant risk factor (OR, 1.005; 95% CI, 1.002–1.009; $P = .004$) (Table 4).

We conducted a 10-fold cross-validation to prove the statistical power of adding LFI to the R₂eD and VALE models. Both models showed improvement in terms of AUC, accuracy, specificity, and other aspects (Table 5).

These results suggest that the addition of LFI to the previous models substantially enhances their predictive performance in assessing outcomes related to AVMs.

DISCUSSION

In this QDSA-based investigation, we undertook a comprehensive examination of hemodynamic characteristics associated with AVM rupture. Our study unearthed a robust association

Table 2: Comparison of angioarchitecture and hemodynamics between the unruptured and ruptured AVMs

Characteristics	Unruptured	Ruptured	P Value
No. of patients	77	103	
Mean nidus volume (mean) (mL)	40.2 (SD, 46.4)	13.6 (SD, 21.0)	<.001 ^a
Angioarchitecture			
Feeding artery dilation	57 (74.0%)	51 (49.5%)	.001 ^a
Single feeding artery	12 (15.6%)	35 (34.0%)	.003 ^a
Deep venous drainage	17 (22.1%)	38 (36.9%)	.035 ^a
Single draining vein	33 (42.9%)	65 (63.1%)	.07
Drainage vein stenosis	11 (14.3%)	27 (26.2%)	.07
Diffuse nidus	15 (19.5%)	38 (36.9%)	.01 ^a
Flow-related aneurysm	14 (18.2%)	43 (41.7%)	.001 ^a
Hemodynamics			
Feeding artery			
TTP (mean) (sec)	2.88 (SD, 0.80)	3.14 (SD, 1.01)	.07
FWHM (mean) (sec)	2.83 (SD, 1.02)	3.33 (SD, 1.29)	.006 ^a
Inflow gradient (mean)	1265.61 (SD, 912.53)	1317.85 (SD, 1018.43)	.72
Outflow gradient (mean)	636.89 (SD, 505.72)	600.35 (SD, 511.84)	.63
Stasis index (mean)	2.42 (SD, 0.99)	2.63 (SD, 1.04)	.16
Drainage vein			
TTP (mean) (sec)	3.62 (SD, 1.07)	3.76 (SD, 1.30)	.42
FWHM (mean) (sec)	3.00 (SD, 0.75)	3.56 (SD, 1.29)	<.001 ^a
Inflow gradient (mean)	1854.28 (SD, 2794.89)	1289.84 (SD, 975.82)	.06
Outflow gradient (mean)	741.99 (SD, 568.85)	610.58 (SD, 522.51)	.11
Stasis index (mean)	2.38 (SD, 0.65)	2.52 (SD, 0.97)	.28
MTT (ICA-sinus) (mean) (sec)	1.48 (SD, 1.03)	1.97 (SD, 1.70)	.02 ^a
MTT (feeding-draining) (mean) (sec)	0.73 (SD, 0.97)	0.62 (SD, 1.04)	.47
ADW (mean)	695.02 (SD, 607.38)	742.75 (SD, 720.42)	.64
TRV (mean)	225.35 (SD, 211.26)	115.93 (SD, 157.39)	<.001 ^a
LFI (mean)	49.40 (SD, 98.25)	390.27 (SD, 919.81)	<.001 ^a

^a Statistical significance ($P < .05$).

Table 3: Univariate and multivariate logistic regression analyses of LFI and 3 LFI-combined models of factors associated with rupture in AVMs

	Univariable Analysis		Angioarchitecture Model		Hemodynamic Model		Combined Model	
	OR (95% CI)	P Value	OR (95% CI)	P Value	OR (95% CI)	P Value	OR (95% CI)	P Value
LFI	1.007 (1.003–1.010)	.001 ^a	1.004 (1.001–1.008)	.02 ^a	1.005 (1.001–1.009)	.009 ^a	1.004 (1.000–1.007)	.03 ^a
Mean nidus volume			0.979 (0.964–0.994)	.007 ^a			0.959 (0.931–0.988)	.005 ^a
Angioarchitecture								
Feeding artery dilation			1.047 (0.443–2.472)	.92			1.028 (0.429–2.461)	.95
Single feeding artery			0.783 (0.299–2.049)	.62			1.112 (0.768–1.608)	.57
Deep venous drainage			2.315 (1.018–6.947)	.05 ^a			2.684 (1.132–6.361)	.03 ^a
Diffuse nidus			2.863 (1.180–6.947)	.02 ^a			2.990 (1.114–8.022)	.03 ^a
Flow-related aneurysm			3.417 (1.521–7.678)	.003 ^a			3.617 (1.544–8.474)	.003 ^a
Hemodynamic								
Feeding artery								
FWHM (sec)					1.067 (0.703–1.619)	.76	0.949 (0.590–1.524)	.83
Drainage vein								
FWHM (sec)					1.218 (0.750–1.978)	.43	1.171 (0.695–1.974)	.55
MTT (ICA-sinus)					1.084 (0.811–1.448)	.59	1.297 (0.933–1.803)	.12
TRV					0.999 (0.997–1.001)	.26	1.004 (0.999–1.009)	.14

^a Statistical significance ($P < .05$).

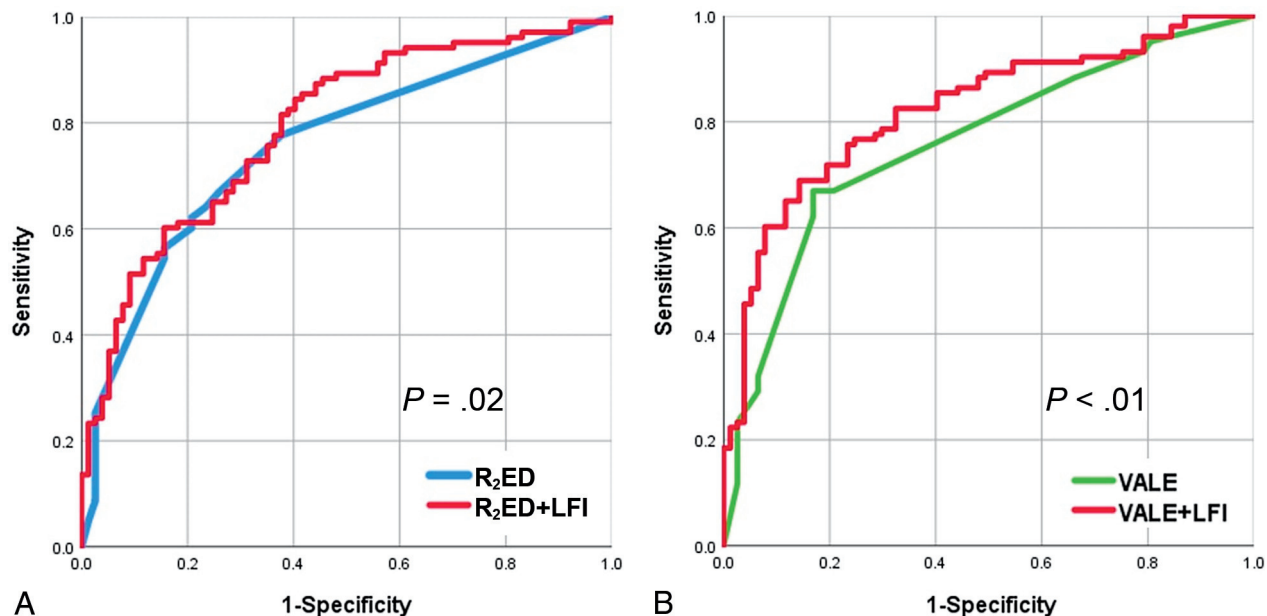


FIG 3. Comparison of 2 AVM rupture-prediction models before and after the inclusion of the LFI. A, Comparing R₂ED and R₂ED+LFI reveals that the original R₂ED AUC value is 0.755. After the inclusion of LFI, the AUC value increases to 0.791. Based on the DeLong test, the significance level is $P = .03$. B, Comparing VALE and VALE+LFI reveals that the original VALE AUC value is 0.760. After the inclusion of LFI, the AUC value increases to 0.823. Based on DeLong test, the significance level is $P = .005$.

Table 4: Performance of previous models after the addition of LFI

Model	AUC (95% CI)	P Value	LFI (95% CI)	P Value
R ₂ eD	0.755 (0.684–0.826)	Reference	Reference	Reference
R ₂ eD + LFI	0.791 (0.725–0.857)	.03 ^a	1.004 (1.000–1.008)	.04 ^a
VALE	0.760 (0.689–0.831)	Reference	Reference	Reference
VALE + LFI	0.823 (0.762–0.884)	.005 ^a	1.005 (1.002–1.009)	.004 ^a

^a Statistical significance ($P < .05$).

Table 5: 10-fold cross-validation of performance with 2 previous models after incorporating LFI

Model	AUC (95%CI)	P Value	Accuracy	Precision	Sensitivity	Specificity
R ₂ eD	0.601 (0.515–0.687)	Reference	0.611	0.674	0.621	0.597
R ₂ eD + LFI	0.624 (0.541–0.707)	.15	0.639	0.702	0.641	0.636
VALE	0.603 (0.518–0.688)	Reference	0.556	0.610	0.621	0.468
VALE + LFI	0.706 (0.629–0.783)	<.001 ^a	0.683	0.717	0.738	0.610

^a Statistical significance ($P < .05$).

between the hemodynamic parameter LFI and the occurrence of AVM rupture, signifying the extent of vascular filling within the lesion. Furthermore, we integrated the LFI into existing AVM rupture-prediction models, and this integration notably bolstered the predictive performance of these models. This outcome reconfirms the significant role of intravascular stasis and obstructive congestion as potential mechanisms contributing to AVM rupture. It also underscores the potential utility of incorporating hemodynamic parameters in the construction of multimodal prediction models, offering the prospect of improved accuracy in forecasting future AVM ruptures.

Owing to the intricate architecture of AVM lesions, prior investigations have often overlooked hemodynamic analysis of AVM niduses, primarily focusing on the feeding arteries or

draining veins. For example, Lin et al⁹ established a correlation between the Stasis Index of the principal draining vein and AVM rupture, Spetzler et al³ associated elevated intravascular pressure in feeding arteries with AVM rupture, and Chen et al¹¹ identified a significant relationship between the TTP ratio of feeding arteries and draining veins and AVM microbleeds. Nevertheless, the primary and most immediate site of AVM rupture is the AVM lesion itself, the anomalous niduslike structure. This lesion stands as the pivotal and direct site for understanding the hemodynamic mechanisms of AVM rupture. Regrettably, due to the intricate vascular architecture inherent in

AVM lesions, techniques such as hemodynamic simulation, intravascular pressure measurement, and transcranial Doppler ultrasound are often not applicable for lesion analysis.

In a preceding study, Chen et al⁶ pioneered an innovative method rooted in QDSA to directly assess the hemodynamic attributes of AVM lesions, proposing that TRV could signify the degree of intravascular stasis within the lesion. However, this study encountered several limitations, including measurement errors attributable to the complex 3D structure of the lesion and an ambiguous interpretation of the meaning of FWHM. In this study, we introduce a novel parameter, the LFI, also founded on QDSA. LFI is derived from the ADW, a metric that reflects blood filling within the ROI and is subsequently normalized by volume. The LFI constitutes the second hemodynamic parameter

developed for the explicit characterization of intravascular stasis within AVM lesions.

The LFI takes inspiration from previous hemodynamic research conducted in DSA and MR imaging.^{16,20,21} At present, hemodynamic indices derived from QDSA focus more on the analysis of ROI curves, because certain mathematic characteristics within these curves could reflect the blood-flow condition.^{13,22,23} In contrast, there are notable gaps in research pertaining to the AUC of ROIs. In QDSA, the AUC is typically regarded as the volume of contrast agent passing through the ROIs, serving as an indirect measure of blood-flow volume. In our exploration of the AUC, we drew inspiration from the concept of the ADW, as defined by Raoult et al.²⁴ and Kramer et al.²⁵ In their research, ADW is defined as a specified time window that theoretically represented good arterial filling with no significant venous contamination. We hypothesize that during the time window represented by ADW, the AVM nidus undergoes maximal blood inflow throughout the entire “inflow-outflow” process. This hypothesis suggests that during this specific period, the perfusion pressure within the nidus exceeds that of other time intervals. The numeric value of the ADW, corresponding to the difference in AUC between arterial and venous phases, is presumed to reflect the discrepancy in blood flow between arteries and veins. A larger ADW indicates a more substantial difference in blood flow between these 2 vascular components. However, as shown in Table 2, there is no statistically significant difference in the ADW between the ruptured and non-ruptured groups. By examining the ROI as well as relevant factors affecting AUC, we found that it is necessary to combine this hemodynamic with some fundamental characteristics of AVM to enhance its specificity in discriminating ruptured cases. In fact, nidus volume is the most significant factor affecting the AUC, and ADW represents the maximum filling in the ROI. Therefore, the maximum filling degree per unit volume of the lesion can be calculated by dividing the ADW by the nidus volume—that is, the LFI (ADW/volume [nidus]). In this context, we contend that LFI represents the maximum perfusion pressure endured by the lesion within a unit volume. A higher LFI suggests an elevated risk of rupture.

Volume is a key parameter in the LFI calculation process. However, the question of whether AVM volume contributes to the risk of rupture remains debated within the academic community.^{18,26–29} In this study, data revealed an association between smaller lesions and rupture. To mitigate the impact of lesion volume on the results, we attempted to normalize the results obtained from the ADW by dividing them by the lesion volume, yielding a unit volume blood-filling index amenable to cross-case comparison. This concept is reminiscent of the TRV, in which lower TRV values were correlated with higher Stasis Indices, indicating sluggish blood flow within AVM lesions. TRV is derived by dividing the FWHM by the maximum diameter of the AVM. Similar to our study, a trend of smaller lesion sizes in the ruptured group was observed, thereby leading us to postulate that the LFI and TRV both reflect, to some extent, blood volume filling and stasis within the lesion.

Stasis of blood within AVM lesions may potentially lead to rupture, with underlying mechanisms likely involving chronic mechanical stress exerted on the vessel walls, triggering inflammatory responses and subsequent endothelial damage, diminished

deformability, and causing eventual rupture.^{11,30,31} Studies by Fry³² demonstrated the impact of shear stress on flow-related changes in venous endothelial cells, while Frösen et al.³¹ established that high wall shear stress conditions activate proinflammatory signaling pathways within vascular endothelial cells, driving remodeling in unruptured intracranial aneurysms. Within our study, this mechanism of rupture is reflected by an elevated LFI, signifying greater unit volume of blood filling.

Univariate analysis indicated that the arterial Stasis Index, TRV, and LFI all demonstrated statistical differences between the 2 groups; however, in multivariate analysis, only LFI remained statistically significant. Consequently, we posit that all 3 parameters mentioned above exert some influence on rupture, yet LFI is the most sensitive indicator with the greatest discriminatory capacity. We attribute this phenomenon to 2 parameters used in the calculation of LFI. We have incorporated volume and the ADW, both of which have been established in multiple studies as having distinct differentiating significance for filling and rupture. The synergy of these 2 parameters amplifies the credibility and discriminative capability of LFI. In further research, our goal is to substantiate the reliability and precision of LFI using more direct measurement techniques, including computational fluid dynamics modeling of the lesion or direct perfusion pressure measurement.

According to the definition of ADW, we believe it reflects the degree of blood-flow filling within the AVM nidus during a specified time window. However, it lacks quantifiability and comparability across cases. Therefore, we attempted to normalize the ADW by dividing it by the volume of the AVM lesion, resulting in a quantitative metric to assess the degree of blood filling within the lesion. Due to the cross-sectional nature of this study, long-term follow-up results for patients with nonruptured AVMs with high LFI levels are unavailable. However, the results demonstrate statistically significant differences in LFI levels among patients with ruptured AVMs, aligning with our hypothesis of a correlation between high perfusion within the lesion volume and rupture. Therefore, we aim to conduct future prospective cohort studies to confirm the predictive ability of LFI for rupture occurrence.

In this study, a comprehensive evaluation of baseline characteristics, angioarchitecture, and hemodynamic features revealed several key insights. Angioarchitecture characteristics differed between the ruptured and unruptured groups, with factors such as feeding artery dilation, single feeding artery, deep venous drainage, single draining vein, drainage vein stenosis, diffuse nidus, and flow-related aneurysms demonstrating significant associations with rupture risk. Hemodynamic parameters, including TTP, MTT, FWHM, ADW, TRV, Stasis Index, and LFI, were also evaluated. While some differences in these parameters were observed, LFI stood out as a robust risk factor of AVM rupture.

Study Limitations

This study has certain limitations. First, the analysis for all enrolled patients was conducted postadmission, and ruptured AVMs may exhibit temporal variations in vascular architecture and hemodynamics. These changes could impact the reliability of the conclusions. Therefore, future research will require a larger sample of patients with prerupture imaging and long-term follow-up observations. Second, QDSA is based on 2D imaging,

which may have limitations such as overlapping structures. Further research using 3D and 4D imaging for hemodynamic analysis may provide a more accurate reflection of pressure within the lesion. Third, this study relied on cross-sectional data, introducing the potential for selection bias to impact the findings. Moreover, the emphasis of the study is on revealing the correlation between LFI and AVM rupture, rather than establishing predictive capabilities or causal relationships. This limitation restricts the direct clinical applicability of the study's results. To bolster the reliability and robustness of the findings, further validation with a larger prospective cohort is imperative.

CONCLUSIONS

In this cross-sectional study, we discovered that a high-filling state of AVM lesions, indicated by elevated LFI levels, is associated with rupture. This association could be a result of excessive arterial perfusion, and it is necessary to evaluate QDSA hemodynamic parameters in the assessment of AVM rupture risk.

ACKNOWLEDGMENTS

We would like to express our gratitude to Beijing Tiantan Hospital for their technical support in this research.

Disclosure forms provided by the authors are available with the full text and PDF of this article at www.ajnr.org.

REFERENCES

- Abecassis IJ, Xu DS, Batjer HH, et al. **Natural history of brain arteriovenous malformations: a systematic review.** *Neurosurg Focus* 2014;37:E7 [CrossRef Medline](#)
- Rutledge C, Cooke DL, Hetts SW, et al. **Brain arteriovenous malformations.** *Handb Clin Neurol* 2021;176:171–78 [CrossRef Medline](#)
- Spetzler RF, Hargraves RW, McCormick PW, et al. **Relationship of perfusion pressure and size to risk of hemorrhage from arteriovenous malformations.** *J Neurosurg* 1992;76:918–23 [CrossRef Medline](#)
- Stapf C, Mast H, Sciacca RR, et al. **Predictors of hemorrhage in patients with untreated brain arteriovenous malformation.** *Neurology* 2006;66:55–55 [CrossRef Medline](#)
- Burkhardt JK, Chen X, Winkler EA, et al. **Delayed venous drainage in ruptured arteriovenous malformations based on quantitative color-coded digital subtraction angiography.** *World Neurosurg* 2017;104:619–27 [CrossRef Medline](#)
- Chen Y, Chen P, Li R, et al. **Rupture-related quantitative hemodynamics of the supratentorial arteriovenous malformation nidus.** *J Neurosurg* 2023;138:740–49 [CrossRef Medline](#)
- Li Z, Chen Y, Chen P, et al. **Quantitative evaluation of hemodynamics after partial embolization of brain arteriovenous malformations.** *J Neurointerv Surg* 2021;14:1112–17 [CrossRef Medline](#)
- Hu YS, Lee CC, Wu HM, et al. **Stagnant venous outflow predicts brain arteriovenous malformation obliteration after gamma knife radiosurgery without prior intervention.** *Neurosurgery* 2020;87:338–47 [CrossRef Medline](#)
- Lin TM, Yang HC, Lee CC, et al. **Stasis index from hemodynamic analysis using quantitative DSA correlates with hemorrhage of supratentorial arteriovenous malformation: a cross-sectional study.** *J Neurosurg* 2019;132:1574–82 [CrossRef Medline](#)
- Lin CJ, Chen KK, Hu YS, et al. **Quantified flow and angioarchitecture show similar associations with hemorrhagic presentation of brain arteriovenous malformations.** *J Neuroradiol* 2023;50:79–85 [CrossRef Medline](#)
- Chen X, Cooke DL, Saloner D, et al. **Higher flow is present in unruptured arteriovenous malformations with silent intrasession microhemorrhages.** *Stroke* 2017;48:2881–84 [CrossRef Medline](#)
- Li R, Chen P, Han H, et al. **Association of nidus size and rupture in brain arteriovenous malformations: Insight from angioarchitecture and hemodynamics.** *Neurosurg Rev* 2023;46:216 [CrossRef Medline](#)
- Wang J, Cheng JJ, Huang KY, et al. **Quantitative assessment of angiographic perfusion reduction using color-coded digital subtraction angiography during transarterial chemoembolization.** *Abdom Radiology (NY)* 2016;41:545–52 [CrossRef Medline](#)
- Atkinson RP, Awad IA, Batjer HH, et al; Joint Writing Group of the Technology Assessment Committee American Society of Interventional and Therapeutic Neuroradiology; Joint Section on Cerebrovascular Neurosurgery a Section of the American Association of Neurological Surgeons and Congress of Neurological Surgeons; Section of Stroke and the Section of Interventional Neurology of the American Academy of Neurology. **Reporting terminology for brain arteriovenous malformation clinical and radiographic features for use in clinical trials.** *Stroke* 2001;32:1430–42 [CrossRef Medline](#)
- Lv X, Wu Z, Jiang C, et al. **Angioarchitectural characteristics of brain arteriovenous malformations with and without hemorrhage.** *World Neurosurg* 2011;76:95–99 [CrossRef Medline](#)
- Dautry R, Edjlali M, Roca P, et al. **Interest of HYPR flow dynamic MRA for characterization of cerebral arteriovenous malformations: comparison with TRICKS MRA and catheter DSA.** *Eur Radiol* 2015;25:3230–37 [CrossRef Medline](#)
- Todaka T, Hamada J, Kai Y, et al. **Analysis of mean transit time of contrast medium in ruptured and unruptured arteriovenous malformations: a digital subtraction angiographic study.** *Stroke* 2003;34:2410–14 [CrossRef Medline](#)
- Feghali J, Yang W, Xu R, et al. **R₂eD AVM score.** *Stroke* 2019;50:1703–10 [CrossRef Medline](#)
- Chen Y, Han H, Meng X, et al. **Development and validation of a scoring system for hemorrhage risk in brain arteriovenous malformations.** *JAMA Netw Open* 2023;6:e231070 [CrossRef Medline](#)
- Benson JC, Chiu S, Flemming K, et al. **MR characteristics of unruptured intracranial arteriovenous malformations associated with seizure as initial clinical presentation.** *J Neurointerv Surg* 2020;12:186–91 [CrossRef Medline](#)
- Scharf J, Brauherr E, Forsting M, et al. **Significance of haemorrhagic lacunes on MRI in patients with hypertensive cerebrovascular disease and intracerebral haemorrhage.** *Neuroradiology* 1994;36:504–08 [CrossRef Medline](#)
- Chen CW, Wong HF, Ye YL, et al. **Quantitative flow measurement after placing a flow diverter for a distal internal carotid artery aneurysm.** *J Neurointerv Surg* 2017;9:1238–42 [CrossRef Medline](#)
- Chen Y, Ma L, Yang S, et al. **Quantitative angiographic hemodynamic evaluation after revascularization surgery for moyamoya disease.** *Transl Stroke Res* 2020;11:871–81 [CrossRef Medline](#)
- Raoult H, Bannier E, Maurel P, et al. **Hemodynamic quantification in brain arteriovenous malformations with time-resolved spin-labeled magnetic resonance angiography.** *Stroke* 2014;45:2461–64 [CrossRef Medline](#)
- Kramer H, Michaely HJ, Requardt M, et al. **Effects of injection rate and dose on image quality in time-resolved magnetic resonance angiography (MRA) by using 1.0M contrast agents.** *Eur Radiol* 2007;17:1394–402 [CrossRef Medline](#)
- Kim H, Salman RA, McCulloch CE, et al; MARS Coinvestigators. **Untreated brain arteriovenous malformation.** *Neurology* 2014;83:590–97 [CrossRef Medline](#)
- Hernesniemi JA, Dashti R, Juvela S, et al. **Natural history of brain arteriovenous malformations: a long-term follow-up study of risk of hemorrhage in 238 patients.** *Neurosurgery* 2008;63:823 [CrossRef Medline](#)
- Ai X, Ye Z, Xu J, et al. **The factors associated with hemorrhagic presentation in children with untreated brain arteriovenous malformation: a meta-analysis.** *J Neurosurg Pediatr* 2018;23:343–54 [CrossRef Medline](#)

29. Chen Y, Meng X, Ma L, et al. **Contemporary management of brain arteriovenous malformations in mainland China: a Web-based nationwide questionnaire survey.** *Chin Neurosurg J* 2020;6:26 [CrossRef Medline](#)
30. Kim H, Su H, Weinsheimer S, et al. **Brain arteriovenous malformation pathogenesis: a response-to-injury paradigm.** *Acta Neurochir Suppl* 2011;111:83–92 [CrossRef Medline](#)
31. Frösen J, Cebal J, Robertson AM, et al. **Flow-induced, inflammation-mediated arterial wall remodeling in the formation and progression of intracranial aneurysms.** *Neurosurg Focus* 2019;47:E21 [CrossRef Medline](#)
32. Fry DL. **Acute vascular endothelial changes associated with increased blood velocity gradients.** *Circ Res* 1968;22:165–97 [CrossRef Medline](#)